Dynamics of superconducting order parameter through ultrafast normal-to-superconducting phase transition in $Bi_2Sr_2CaCu_2O_{8+\delta}$ from multipulse polarization-resolved transient optical reflectivity

I. Madan,[1,2] V. V. Baranov,[1] Y. Toda,[3] M. Oda,[4] T. Kurosawa,[4] V. V. Kabanov,[1] T. Mertelj,[1,5,*] and D. Mihailovic[1,5]

[1]*Complex Matter Department, Jozef Stefan Institute, Jamova 39, 1000 Ljubljana, Slovenia*

[2]*Laboratory for Ultrafast Microscopy and Electron Scattering, IPHYS, École Polytechnique Fédérale de Lausanne, CH-1015 Lausanne, Switzerland*

[3]*Department of Applied Physics, Hokkaido University, Sapporo 060-8628, Japan*

[4]*Department of Physics, Hokkaido University, Sapporo 060-0810, Japan*

[5]*Center of Excellence on Nanoscience and Nanotechnology Nanocenter (CENN Nanocenter), Jamova 39, 1000 Ljubljana, Slovenia*

(Received 29 June 2017; revised manuscript received 13 October 2017; published 27 November 2017)

A systematic temperature-dependent study of the femtosecond optical superconducting (SC) state destruction and recovery in $Bi_2Sr_2CaCu_2O_{8+\delta}$ cuprate superconductor by means of the all-optical polarization-sensitive multipulse spectroscopy is presented. At low temperatures and a partial SC state suppression, an anisotropic SC-gap recovery time scale is suggested by the data. The SC state destruction and recovery dynamics are compared to the recent TR-ARPES-inferred SC-gap dynamics and a qualitative agreement is found. Using a phenomenological response function, the experimental data are also compared to time-dependent Ginzburg-Landau model simulations.

DOI: 10.1103/PhysRevB.96.184522

I. INTRODUCTION

The study of the time evolution of complex systems through symmetry-breaking transitions (SBT) is of great fundamental interest in different areas of physics [1–3]. An SBT of particular general interest is the ultrafast normal-to-superconducting (N → S) state transition. Due to the small heat capacity of the electronic system, an optical pulse can efficiently suppress the SC state without heating the low-frequency phonon heat bath, which remains well below the critical temperature (T_c). This enables us to perform an ultrafast effective[1] electron temperature quench across T_c with an ultrashort laser pulse, which is then followed by an ultrafast nonequilibrium N → S transition.

The ultrafast S → N → S transition in the cuprate superconductors has been initially studied by all-optical [4–8] pump-probe technique followed by laser ARPES [9–12]. While the laser ARPES can directly resolve the momentum-dependent[2] quasiparticle (QP) distribution function, all-optical techniques offer better bulk sensitivity and greater flexibility. The lack of momentum resolution of an optical probe can be partially compensated by use of the optical dipole transition selection rules that depend on the probe-photon polarization [13,14] and energy [7,15] and enable selection of different parts of the Brillouin zone (BZ).

The electronic Raman-scattering tensor analyses have shown [13] that the dielectric tensor fluctuations of different symmetries can be linked to charge excitations in different parts of the BZ. In particular, in a D_{4h} point-symmetry corresponding to the ideal CuO_2-plane symmetry, the dielectric tensor fluctuations with the B_{1g} and B_{2g} symmetries are linked to the antinodal and nodal BZ charge excitations, respectively, while the totally symmetric A_{1g} fluctuations do not discriminate between the regions. The transient reflectivity ΔR is related to the Raman tensor and in $Bi_2Sr_2CaCu_2O_{8+\delta}$ (Bi-2212) the B_{1g}-like[3] transient reflectivity component shows sensitivity to the SC state only, while A_{1g}-like and B_{2g}-like transient reflectivity components couple to both the SC and pseudogap (PG) order [14].

While the all-optical transient response in the cuprates under weak excitation can be well described in terms of the photoinduced absorption of the photoexcited quasiparticles [16], the response function in highly nonequilibrium states is unclear due to unknown relative contributions of collective and single-particle degrees of freedom to the transient optical reflectivity. To overcome this problem, the standard two-pulse all-optical pump-probe technique was extended to a multipulse technique, which was shown to be instrumental in extracting the order-parameter dynamics in a charge density wave compound [17] as well as in the prototypical cuprate superconductor $La_{1.9}Sr_{0.1}CuO_4$ [18].

Here, we extend our previous study [18] of an ultrafast S → N → S transition in $La_{1.9}Sr_{0.1}CuO_4$ to $Bi_2Sr_2CaCu_2O_{8+\delta}$ in search of universality, and also to uncover potential important differences in the two materials with substantially different critical temperatures and pseudogap/SC-gap ratios. By means of the all-optical multipulse technique combined with the polarization-selective optical probe, we were able to separate the SC state recovery dynamics from the previously studied [19] PG state recovery dynamic and enable discrimination between relaxation in the nodal and antinodal BZ regions. The material has been studied previously by time-resolved techniques [6,7,9–11,20], but thus far there has been no systematic study of the nonequilibrium transitions in this material, especially by the three-pulse technique.

*tomaz.mertelj@ijs.si

[1]The quasiparticle energy distribution is nonthermal, so strictly speaking the electronic T is not well defined.

[2]Limited to the vicinity to the nodal point on the Γ-Y line.

[3]Despite Bi-2212 is orthorhombic, we use the ideal D_{4h} point-group tetragonal CuO_2-plane symmetry to simplify the notation. See Supplemental Material to Ref. [14] for details.

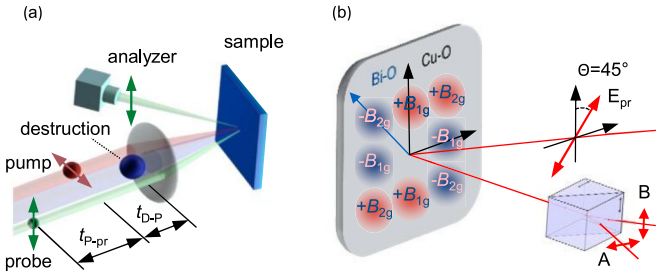

FIG. 1. (a) Schematic representation of the three-pulse experiment and notation of delays between pulses. (b) Schematic representation of the detection of $\Delta R_{B_{1g}}$ using a Wollaston prism. The initial probe polarization is set at 45° with respect to the Cu-O bond direction. The intensity in channels A and B is balanced and the differential signal is recorded, so that all contributions except $\Delta R_{B_{1g}}$ are canceled out.

Our study shows that unlike in $La_{1.9}Sr_{0.1}CuO_4$, where the time-dependent Ginzburg-Landau (TDGL) theory can provide a fair quantitative description of the SC order-parameter recovery, only a qualitative description of the data is possible in Bi-2212, which we attribute to the large SC order fluctuations in the PG state near time of the transition. In addition, when only a partial SC state suppression is achieved, the polarization-resolved optical probe enables us to detect anisotropic SC-order recovery time scales, revealing a faster SC gap recovery in the antinodal direction in comparison with the nodal BZ regions.

II. EXPERIMENT

The sample used in this work was underdoped $Bi_2Sr_2CaCu_2O_{8+\delta}$ (Bi-2212) single crystal with $T_c \approx 78$ K ($\delta = 0.14$) grown by means of the traveling solvent floating zone method. Before mounting into a liquid-He flow cryostat, the sample was freshly cleaved using sticky tape.

The pulse train from a 250-KHz 1.55-eV Ti:sapphire regenerative amplifier was split into 50-fs destruction (D), pump (P), and probe (pr) pulse trains that were independently delayed with respect to each other. The resulting beams were focused and overlapped on the sample [see Fig. 1(a)]. As in the standard pump-probe stroboscopic experiments, the transient reflectivity $\Delta R/R$ was measured by monitoring the intensity of the weakest pr beam. The direct contribution of the unchopped D beam to ΔR was rejected by means of a lock-in synchronized to the chopper that modulated the intensity of the P beam only. The fluences $\mathcal{F}_P < 5$ μJ/cm^2 and $\mathcal{F}_{pr} < 3$ μJ/cm^2 of the P and pr pulses were kept in the linear response region, well below the superconductivity destruction threshold [6,7,21].

To select different components of the anisotropic transient reflectivity [14], two different polarization-sensitive detection schemes were used. In the parallel detection scheme (PDS), which is sensitive to the sum of $\Delta R_{A_{1g}}$ and $\Delta R_{B_{1g}}$ components,[4] $\Delta R = \Delta R_{A_g} + \Delta R_{B_{1g}}$, we used a single photodiode detection with an analyzer parallel to the pr-beam polarization, where the pr-beam polarization was parallel to the Cu-O bond direction. The polarizations of the P and D beams were perpendicular to the pr-beam polarization in order to suppress the signal due to P beam scattering.

In the balanced detection scheme (BDS), which is sensitive to the $\Delta R_{B_{1g}}$ component only, the pr-beam polarization was oriented at 45° with respect to the Cu-O bond directions and two photodiodes in combination with a Wollaston prism were used for detection [see Fig. 1(b)]. When the polarization axes of such detector are oriented along the Cu-O bond directions, the difference of the two photodiode photocurrents corresponds to $\Delta R_{B_{1g}}$, while $\Delta R_{A_{1g}}$ and $\Delta R_{B_{2g}}$ components are rejected. Fine alignment of the polarization and detector angles was done in the PG state at 120 K, to achieve a complete cancellation of the transient PG response.

In order to suppress the P-beam scattering contribution to the signal in the BDS, the P-beam frequency was doubled[5] (3.1-eV P-photon energy) and a long-pass filter in front of the detector was used while the 1.55-eV D-photon energy was the same as in the first scheme.[6]

III. RESULTS

A. SC state destruction

To illustrate the destruction of the SC state, in Fig. 2 we plot the transient reflectivity for the case when the D pulse arrives after the P pulse using the PDS. Depending on the D-pulse fluence $\mathcal{F}_D$, the transient reflectivity is suppressed to different degrees. Above $\mathcal{F}_D \sim 70$ μJ/cm^2, SC order is completely suppressed on a 200-fs time scale after the D-pulse arrival. Above $\mathcal{F}_D \sim 70$ μJ/cm^2 we observe also a small negative overshot lasting a few hundred femtoseconds followed by a weak recovery of the signal on a picosecond time scale. Both features vanish at the highest fluence of ~ 400 μJ/cm^2. The suppression time scale does not depend on the D-pulse arrival time [Fig. 2(b)] nor temperature [Fig. 2(c)].

B. SC state recovery

In Fig. 3 we show a typical transient reflectivity data set measured in the PDS for the case when the P pulse arrives after the D pulse. After a complete suppression for $t_{D\text{-}P} \lesssim 0.5$ ps we first observe a recovery of the negative PG component on a $1 \sim$ ps time scale followed by the recovery of the positive SC component.

As shown previously [14], the PG response does not contribute to $\Delta R_{B_{1g}}$ so recovery of the SC component on the short $t_{D\text{-}P}$ time scale can be observed more clearly in the BDS. In Fig. 4 we show a typical transient reflectivity data set measured using the BDS. As expected, the PG component

[4] As in Ref. [14] we use the approximate notation corresponding to the tetragonal symmetry.

[5] It is generally conjectured that there is no dependence of the transient reflectivity response on the pump-photon energy in the cuprates in the visible photon-energy region. To ensure this conjecture holds for our sample we compared the transient reflectivity in the BDS at $T = 15K$ for 1.55-eV and 3.1-eV pump-photon energies at weak excitation and found no measurable differences.

[6] The scattering from the D beam does not contribute significantly since the beam is not modulated.

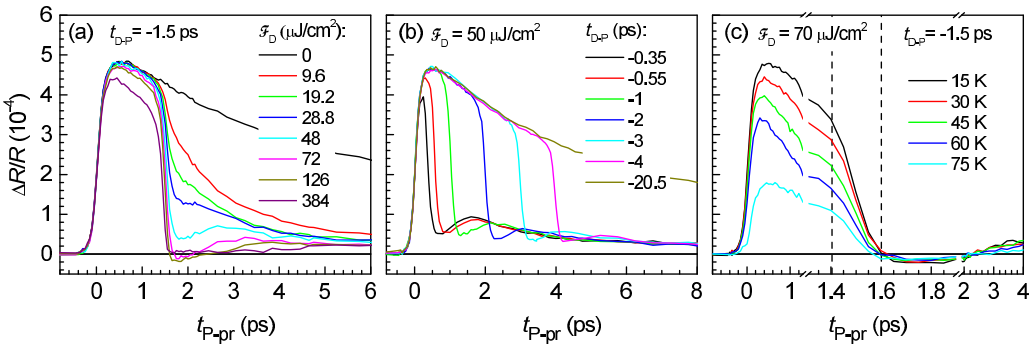

FIG. 2. The influence of the destruction pulse on the transient reflectivity in the superconducting state, when the D pulse arrives after the P pulse using the PDS. (a), (b) Show dependence on the D-pulse fluence and $t_{D\text{-}P}$ delay at $T = 15$ K, respectively. (c) T dependence of the transient reflectivity suppression.

is suppressed, but the signal-to-noise ratio is reduced since $\Delta R_{B_{1g}}$ is an order of magnitude smaller than $\Delta R_{A_{1g}}$.

IV. ANALYSIS AND DISCUSSION

A. SC state destruction

The SC state destruction time scale (upon arrival of the D pulse) of ∼200 fs is temperature and destruction-pulse fluence independent and faster than ∼700 fs in LSCO [5,8]. In LSCO it was suggested [5,8] that the high-energy optical phonons created during the relaxation of the primary photoexcited electron-hole pair are the dominating pair-breaking excitation setting the destruction time scale.

The faster destruction time scale in Bi-2212 does not exclude the same phonon-mediated destruction mechanism since one polar optical phonon can be generated by a photoexcited electron/hole every ∼5 fs [8]. Taking the initial photoelectron/hole energy of ∼1 eV and optical phonon energy of 50 meV leads to ∼100 fs photoelectron/hole energy relaxation time that is fast enough to be compatible with the experimental data [23]. The phonon-dominated pair-breaking destruction of the SC state is supported also by the large optical SC state destruction energy that is five times larger than the SC condensation energy [21].

B. Analysis of the SC state recovery

To analyze the recovery, we first fit a finite-rise-time single-exponential relaxation model to the transient reflectivity in Fig. 4 to obtain the $t_{D\text{-}P}$ dependent relaxation rate γ. In the inset to Fig. 4(a) we compare the relaxation rate γ from the fit to the amplitude of the B_{1g} SC response, $A_{B_{1g}} = \overline{\Delta R_{B_{1g}}}/\overline{\Delta R_{B_{1g},\text{no-D}}}$. Here, $\overline{y}$ corresponds to the average of y in the interval[7] $t_{P\text{-}pr} =$ 0.5–0.7 ps and $\Delta R_{B_{1g},\text{no-D}}$ to the transient reflectivity in the absence of the D pulse.

γ and $A_{B_{1g}}$ initially recover on a similar time scale of ∼4 ps followed by slower dynamics extending towards the nanosecond time scale. As in the case of (La,Sr)$CuO_{4+\delta}$ (LSCO), we attribute the suppression of γ during the first part of the recovery to the critical slowing down of the SC fluctuations in the vicinity of the transition [18]. Upon the initial increase, γ decreases on the nanosecond time scale,

[7]In the vicinity of the peak of the unperturbed $\Delta R_{B_{1g}}/R$ response.

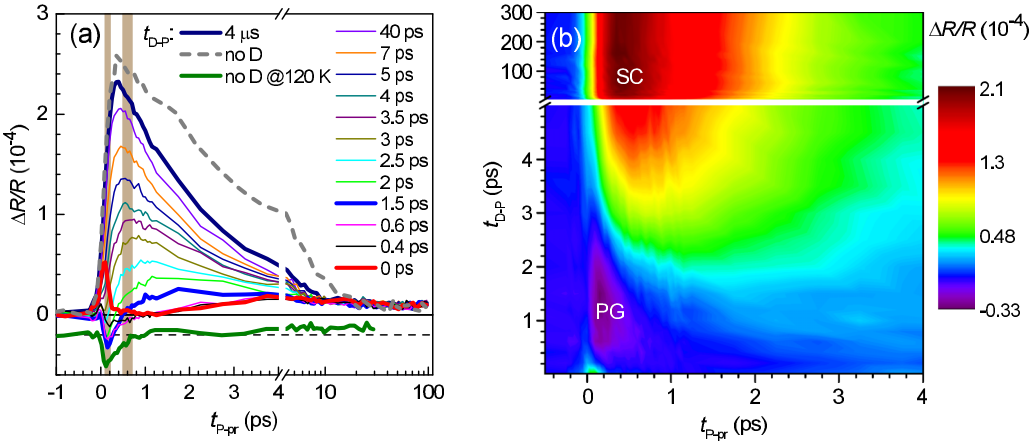

FIG. 3. (a) Transient reflectivity using the PDS at $T = 40$ K with $\mathcal{F}_D = 68\mu$J/cm^2. For comparison, a transient measured in the PG state ($T = 120$ K) in the absence of the D pulse is shown vertically shifted below the main data. The vertical shaded areas indicates the readout $t_{P\text{-}pr}$ delays (see text). (b) The same data set as in (a) shown as a color map. At $t_{D\text{-}P} = 0$ both the PG and SC signals are suppressed. With increasing $t_{D\text{-}P}$ one can observe a sequential recovery of the negative PG response followed by the positive SC response.

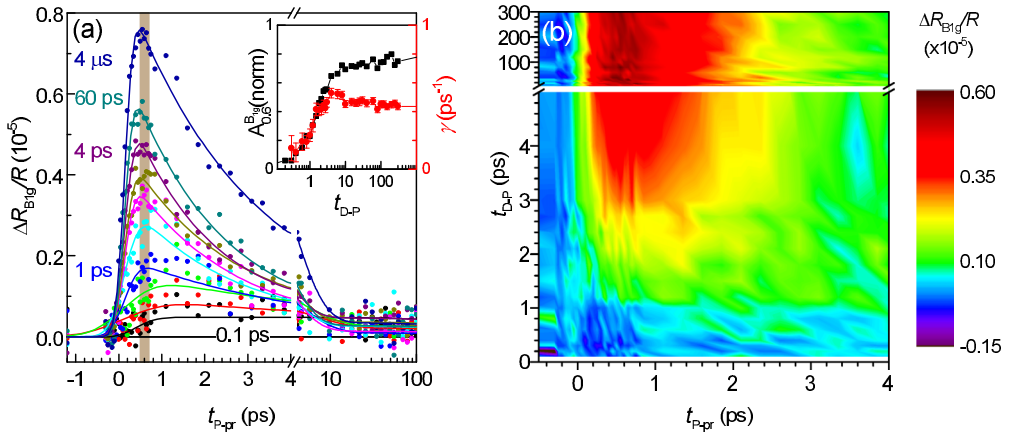

FIG. 4. (a) Recovery of the transient-reflectivity B_{1g} component measured using BDS at $T = 40$ K and $\mathcal{F}_D = 56$ μJ/cm^2. The thin lines are finite-rise-time single-exponential fits [22]. The vertical shaded area represents the interval used to determine A_{SC}. Inset: black squares (left axis), normalized amplitude of the response; red circles, relaxation rate extracted form single-exponential fits to the traces. Error bars are the standard errors of the regression analysis. (b) The same data as in (a) shown as a color map in $t_{D\text{-}P} - t_{P\text{-}pr}$. In the absence of the PG response recovery of the SC signal is evident already at $t_{D\text{-}P} \sim 1$ ps.

indicating cooling of the probed volume: Since the effective temperature on longer time scales is far from the critical temperature, the T dependence of γ is no longer critical but determined by the Rothwarf-Taylor bottleneck dynamics [24].

Contrary to LSCO, where the PG component shows no suppression up to a rather high excitation fluence [25], the PG component in Bi-2212 shows suppression already below [19] $\sim$100 μJ/cm^2 so also the PG component is affected by the D pulse. To extract the SC component recovery dynamics in the PDS, it is therefore necessary to take the PG dynamics into account.

In the standard two-pulse pump-probe experiments, the PG component peaks at $t_{P\text{-}pr} = 0.15$ ps [see Fig. 3(a)]. Traces of $\Delta R/R$ at this $t_{P\text{-}pr}$ as function of $t_{D\text{-}P}$ are shown in Figs. 5(a)–5(c). It is evident that at higher destruction-pulse fluences, the PG recovery leads to nonmonotonous traces due to the sub-ps recovery time scale [19] of the negative PG component preceding the recovery of the positive SC state component.

Due to the rather fast PG-component relaxation time [14] [see Fig. 3(a)], the contribution of the PG component to $\Delta R/R$ should diminish with increasing $t_{P\text{-}pr}$. To avoid the PG recovery contribution, we therefore take $t_{P\text{-}pr}$ in the interval $\{0.5 \text{ ps} < t_{P\text{-}pr} < 0.7 \text{ ps}\}$ where $\Delta R_{B_{1g}}/R$ has a peak[8] in the absence of the D pulse and the PG response is already significantly suppressed to calculate the normalized average $A = \overline{\Delta R/\Delta R_{no\text{-}D}}$, with diminished PG contribution. Indeed, $A(t_{D\text{-}P})$ traces presented in Figs. 5(d)–5(f) show significantly less PG-component recovery and appear very similar to the equivalent $A_{B_{1g}}(t_{D\text{-}P})$ traces shown in Figs. 5(g)–5(i).

At $T > T_c$ the PG state recovers upon destruction on the $\tau_{PG} \sim 0.7$ ps time scale[9] [19]. To check whether the amplitude of the PG component is modified during the slower SC state recovery [15], we compare in Fig. 6 the two readouts with different PG contributions taken at $t_{P\text{-}pr} = 0.15$ ps and the average in the interval $\{0.5 \text{ ps} < t_{P\text{-}pr} < 0.7 \text{ ps}\}$ (A). At the highest $\mathcal{F}_D = 132$ μJ/cm^2 it is possible to overlap the traces beyond $t_{D\text{-}pr} \gtrsim 1$ ps at all measured temperatures when plotted as a function of[10] $t_{D\text{-}pr}$ by vertically shifting[11] and rescaling. At intermediate destruction-pulse fluences the complete overlap is not possible. The shifted and rescaled readouts at $t_{P\text{-}pr} = 0.15$ ps show slightly higher values in the $\sim$2–$\sim$10-ps $t_{D\text{-}P}$-delay range. This could indicate that the negative PG response at 1.55-eV probe-photon energy is transiently suppressed[12] by the appearance of the SC order.

A possibly related suppression of the PG component in the SC state at 1.08-eV probe-photon energy was suggested recently [15]. Considering an earlier report [7], however, where by selecting a particular polarization and probe-photon energy no suppression of the PG component in the SC state was observed, we attribute the difference between readouts in our experiment to the SC-gap-dependent prebottleneck SC state dynamics, which influences the readouts at $t_{P\text{-}pr} = 0.15$ ps.

C. SC state recovery time scale in nodal and antinodal response

The transient reflectivity dynamics in the cuprates is dominated by the quasiparticle-density dynamics while the multipulse technique is sensitive mainly to the collective order-parameter dynamics [17,18]. To investigate the differences between the quasiparticle-density and SC-order dynamics, we compare in Fig. 7(b) the fluence dependencies of the SC recovery time τ_{rec} for both symmetries to the standard two-pulse transient-reflectivity relaxation time[13] τ_{2p}. We estimate

[8]The $A_{1g} + B_{1g}$ $\Delta R/R$ has a peak at a slightly earlier time, where the PG-component contribution is significantly larger.

[9]τ_{PG} is defined by an exponential recovery: $[1 - \exp(-t/\tau_{PG})]$.

[10]The difference in sampling time of 0.55 ps needs to be taken into account when directly comparing the traces.

[11]The fully recovered PG component contributes to a $t_{D\text{-}P}$-independent negative shift at longer $t_{D\text{-}P}$.

[12]When the negative PG component is suppressed, the total $\Delta R/R$ increases.

[13]See the 4-μs trace in Fig. 4(a) for an example fit.

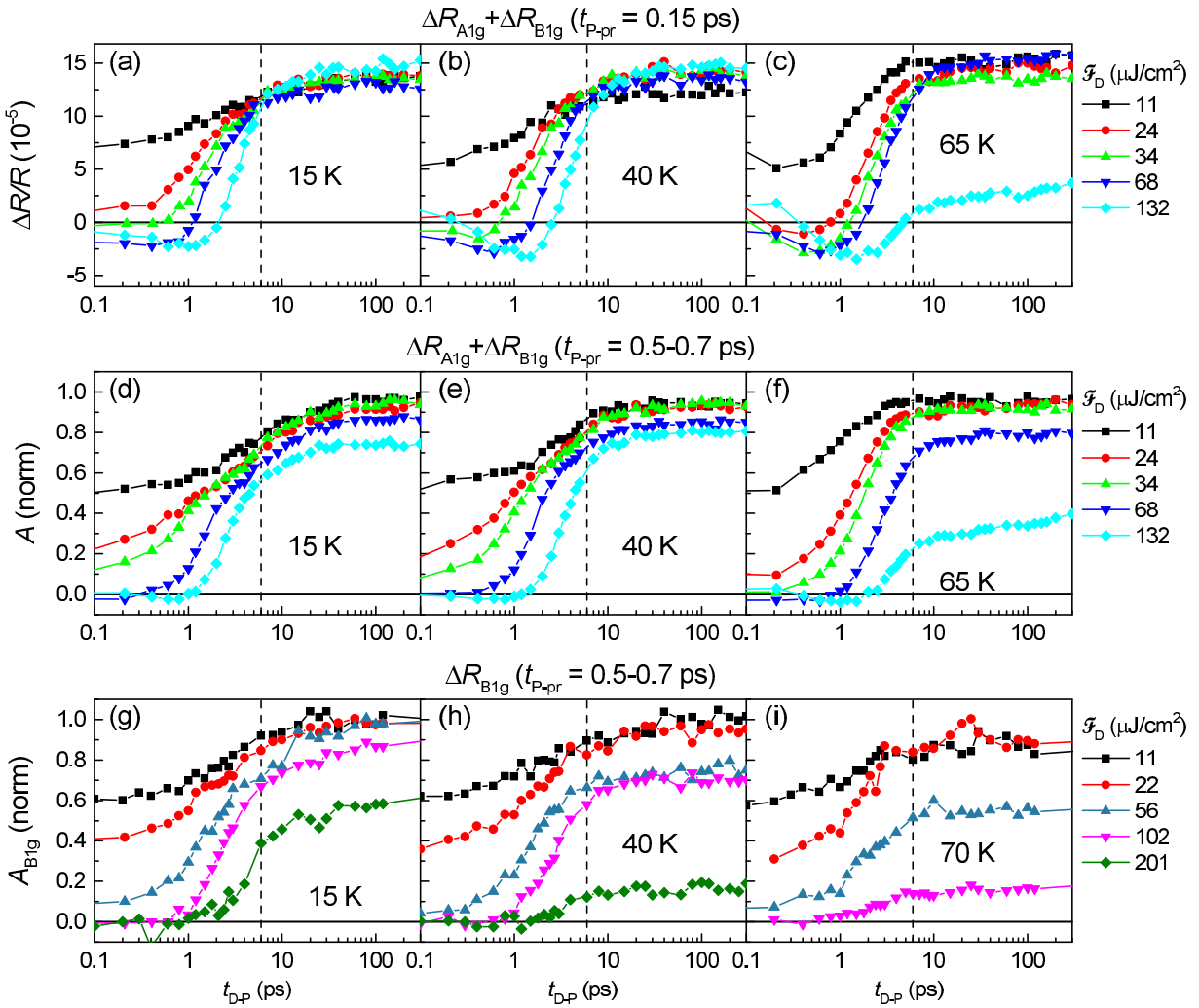

FIG. 5. (a)–(c) The transient reflectivity at $t_{\text{P-pr}} = 0.15$ ps, corresponding to the delay at which the PG response peaks, as a function of $t_{\text{D-P}}$ for different D-pulse fluences at different temperatures. (d)–(f) Evolution of the normalized $\Delta R/R$ amplitude averaged in the 0.5 ps $\leqslant t_{\text{P-pr}} \leqslant$ 0.7 ps range as a function of $t_{\text{D-P}}$ for different D-pulse fluences at different temperatures. (g)–(i) The same for $\Delta R_{B_{1g}}/R$.

τ_{rec} using a phenomenological exponential fit

$$A_{\text{S}} = A_{\text{T}} - A_{\text{e}} e^{-t_{\text{D-P}}/\tau_{\text{rec}}} \tag{1}$$

to the trajectories in Figs. 5(d)–5(i). Here, A_{S} is the normalized three-pulse response amplitude, where A_{T} and A_{e} parameters determine the short- and long-$t_{\text{D-P}}$ amplitude. The lower $\mathcal{F}_{\text{D}}$ data can be rather well fit using this simple single-exponential recovery model (1), while at higher $\mathcal{F}_{\text{D}}$ the recovery appears clearly nonexponential as shown in Fig 7(a).

As a function of fluence both τ_{rec} and $\tau_{2\text{p}}$ show a minimum at intermediate fluences. Above $\mathcal{F}_{\text{D}} \sim 100\ \mu\text{J/cm}^2$, time scales of different signals match rather well[14] and show virtually no T dependence [see Fig. 7(c)]. At low $\mathcal{F}_{\text{D}}$ and $T = 15$ K, however, the A_{1g}-dominated channel τ_{rec} slows down much more with decreasing $\mathcal{F}_{\text{D}}$ than the B_{1g} channel τ_{rec} and $\tau_{2\text{p}}$. On the contrary, at $T = 40$ K, both, the A_{1g}-dominated and B_{1g} channel τ_{rec} show identical fluence dependence in the full $\mathcal{F}_{\text{D}}$ range with a sharp upturn at $\mathcal{F}_{\text{D}} \sim 60\ \mu\text{J/cm}^2$.

A faster $\Delta R/R$ relaxation in the B_{1g} configuration has been observed already in the low-excitation two-pulse experiments [14]. Due to the sensitivity of the the B_{1g} configuration to the antinodal Brillouin-zone (BZ) region, this is consistent with a faster quasiparticle density relaxation around antinodes[15] either by recombination or by scattering into the nodal BZ region, which contributes to the A_{1g}-dominated channel showing a slower decay.

The effect of the faster antinodal quasiparticle relaxation is also evident in our three-pulse experiment, but only when the SC order is not completely suppressed and T is below ~40 K. From the three-pulse data it appears that upon a modest suppression, the SC gap recovers faster at the antinodes than near the nodes.

At higher $\mathcal{F}_{\text{D}}$, upon a complete suppression of the SC gap our data suggest the recovery that is more homogeneous across

[14]Despite the worse fit quality.

[15]A consistent increase of the QP relaxation time away from the nodal point was observed in a recent ARPES experiment [11] in some controversy to an earlier ARPES result [20].

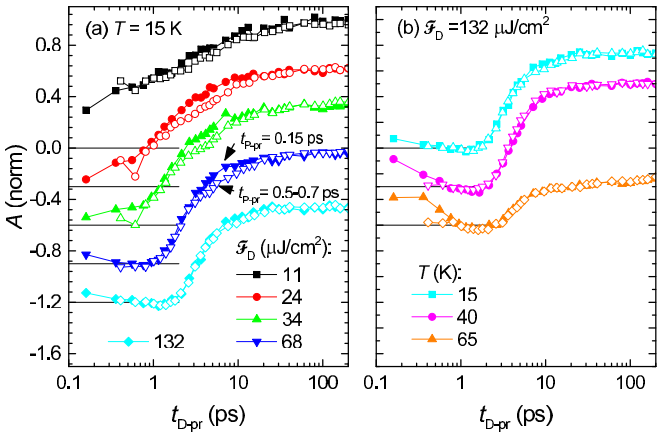

FIG. 6. Comparison of A_S at two different $t_{P\text{-}pr}$ as a function of $t_{D\text{-}pr}$. The traces are vertically shifted for clarity as indicated by the horizontal thin lines. Full and open symbols correspond to $t_{P\text{-}pr} = 0.15$ ps and $t_{P\text{-}pr} = 0.5$–0.7 ps, respectively. The strongly PG-affected ($t_{P\text{-}pr} = 0.15$ ps) traces (full symbols) are vertically shifted and scaled to achieve the best match for $t_{D\text{-}pr} \gtrsim 1$ ps.

the Fermi surface. This could be attributed to two factors. First, during the initial part of the recovery, the suppression of the Rothwarf-Taylor phonon bottleneck [24] and lifting of the SC-gap-imposed QP-relaxation phase-space restrictions [27] enable efficient transfer of the excess QP energy to the phonon bath together with efficient diffusion of excitations across all of the BZ. Second, at higher $\mathcal{F}_D$, the lattice bath is heated closer to T_c so the QP-relaxation phase-space restrictions can be easier overcome by the phonon-assisted QP scattering.

In LSCO [Fig. 7(b)], both τ_{rec} and τ_{2p} are significantly longer than in Bi-2212 [7]. The generally slower τ_{2p} and τ_{rec} in LSCO could be attributed to the smaller SC gap enhancing the quasiparticle relaxation bottleneck [16]. Moreover, in LSCO τ_{rec} increases monotonically above the destruction threshold fluence [5] $\mathcal{F}_{Dth} = 4.2\mu$J/cm^2, while in Bi-2212 with [7] $\mathcal{F}_{Dth} = \sim 16$ μJ/cm^2, the increase starts only above $\sim 4\mathcal{F}_{Dth}$. This could be attributed to the lattice temperature after the quench being closer[16] to T_c in LSCO than in Bi-2212, resulting in a stronger critical slowing down of the SC order-parameter dynamics.

D. Time-dependent Ginzburg-Landau model

We proceed by analyzing the trajectory of the SC amplitude through the transition in the framework of the time-dependent Ginzburg-Landau (TDGL) theory. In the previous study [18] of the SC-order recovery in LSCO we have shown that the TDGL theory fails to consistently describe the ultrafast optical destruction of the SC condensate. On the other hand, *the SC condensate recovery can be quantitatively modeled* using a phenomenological response function and the Ginzburg-Landau time τ_{GL} as the only free fit parameter assuming a finite magnitude of the initial depth-dependent order parameter [Fig. 3(c) in Ref. [18]]. The magnitude of the initial order

[16]In LSCO, the lattice temperature after the destruction pulse reaches [18] T_c at $\mathcal{F}_D = 20$ μJ/cm^2.

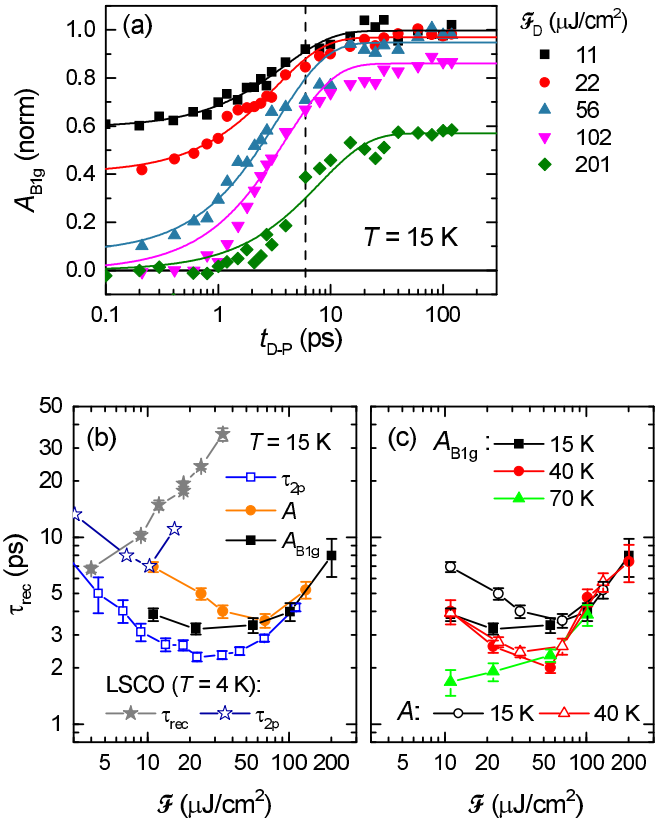

FIG. 7. (a) Fits of Eq. (1) to the $A_{B_{1g}}$ trajectories at $T = 15$ K. (b) The recovery time of the superconducting response from the fits at $T = 15$ K as a function of fluence for $A_{B_{1g}}$ and A trajectories [Figs. 5(d) and 5(g)]. For comparison, the $\Delta R/R$ relaxation time from a two-pulse experiment at 15 K in Bi-2212 is shown by open squares. The corresponding relaxation times in LSCO [26] at $T = 4$ K are shown by stars. (c) Temperature dependence of τ_{rec} of $A_{B_{1g}}$ (full symbols) and A (open symbols) trajectories.

parameter corresponds to the magnitude of the frozen SC fluctuations after the quench from the normal/PG to the SC state which is a function of the depth-dependent quench rate [Eq. (4) in Ref. [18]]. Slower quench rate at higher absorbed energy density implies smaller frozen fluctuations near the sample surface. In LSCO, even better fit is possible using a linear phenomenological depth-dependent initial order parameter $\psi_{BC}(z)$:

$$\psi_{BC}(z) = \begin{cases} c\,z & , U_D(z) > U_{th} \\ \sqrt{1 - T/T_c} & , U_D(z) \leqslant U_{th} \end{cases} \qquad (2)$$

where z is the normal distance form the sample surface and c is an additional $\mathcal{F}_D$-dependent free parameter, $U_D(z)$ the depth-dependent absorbed optical-energy density, and U_{th} the SC destruction-threshold optical-energy density.

In the following, we apply a similar TDGL approach to the SC state recovery dynamics in Bi-2212.

1. *Response function*

As a starting point, one needs to establish the relation between the superconducting order-parameter magnitude $|\psi_{GL}|$ and the transient optical response amplitude. This relation was

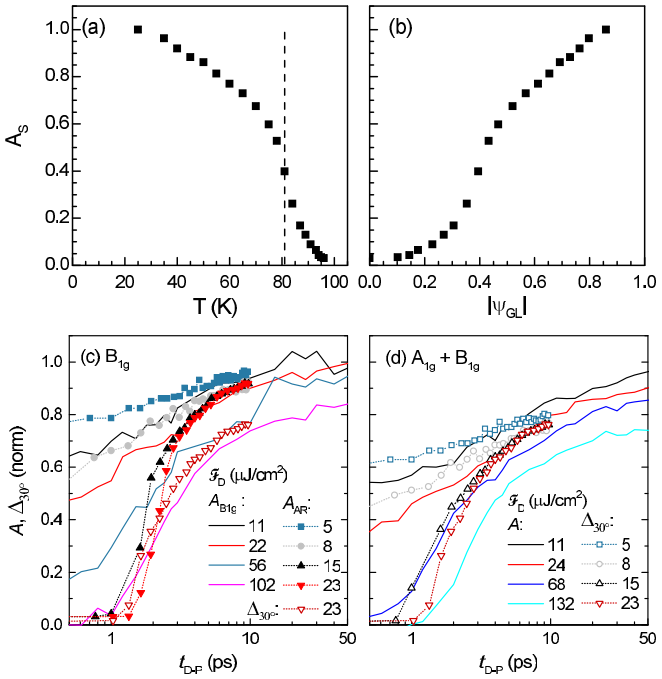

FIG. 8. (a) The amplitude of the normalized transient superconducting response as a function of temperature. The dashed vertical line marks the critical temperature measured by a SQUID magnetometer. (b) The amplitude of the the normalized transient superconducting response as a phenomenological function of the GL order parameter $A_S^{\psi}(|\psi_{GL}|)$, obtained from (a) assuming a mean field $T_c^{MF} = 96$ K. This relation is used as the response function for the theoretical calculation of the superconducting order-parameter evolution presented in Fig. 9. (c) Comparison of $A_{B_{1g}}$ to A_{AR} obtained form the TR-ARPES gap dynamics [10] using the response function from (b). The normalized TR-ARPES gap (open symbols) at the highest $\mathcal{F}_{ARPES}$ is also shown for comparison. (d) Comparison of $A_{0.6}$ to to the normalized TR-ARPES gap.

in the case of LSCO established phenomenologically from the temperature dependence of the normalized weak-excitation $\Delta R/R$ amplitude A_S [18].

In Bi-2212, A_S does not go to zero at T_c due to the large pairing fluctuations [28,29] above T_c as shown in Fig. 8(a), inconsistently with the the GL theory. However, by taking into account that A_S is sensitive to the pairing amplitude [29] and not the SC phase coherence, we can still apply the GL description assuming that only the SC phase coherence is established at T_c, while the largest temperature at which A_S is still observable corresponds to the mean-field pairing critical temperature $T_c^{MF} \simeq 96$ K. Implying the standard GL T dependence of the (pairing) order parameter

$$|\psi_{GL}(T)| \propto \sqrt{1 - T/T_c^{MF}}, \tag{3}$$

we establish a link between A_S and $|\psi_{GL}|$ assuming that at the weak excitation A_S depends on temperature only through the order parameter $A_S(T) = A_S^{\psi}[|\psi_{GL}(T)|]$. We can now establish the response function $A_S^{\psi}(|\psi_{GL}|)$ from experimental $A_S(T)$ assuming $A_S^{\psi}(|\psi_{GL}|) = A_S[T(|\psi_{GL}|)]$ where $T(|\psi_{GL}|)$ is obtained by inverting Eq. (3), as shown in Figs. 8(a) and 8(b).

To further analyze the link between the SC order parameter and A_S, we compare our results to recent TR-ARPES gap dynamics data in near-optimally doped Bi-2212 ($T_c = 91$ K) [10]. Considering the different doping levels of the samples and different spatial[17] and reciprocal-space[18] sensitivities of the probes, only a qualitative correspondence between the results is expected since even in the case of TR-ARPES, the extraction of the SC gap is not rigorously defined [10]. For the sake of comparison, we therefore assume that $|\psi_{GL}(t)| \propto \Delta_{30°}(t)$, where $\Delta_{30°}(t)$ corresponds to the TR-ARPES gap at the edge of the Fermi arc and calculate $A_{AR}(t) = A_S^{\psi}[\Delta_{30°}(t)/\Delta_{30°}(\infty)]$ using the response function A_S^{ψ} shown in Fig. 8(b). In Figs. 8(c) and 8(d) we show comparison of our data to both A_{AR} and the normalized TR-ARPES gap $\Delta_{30°}/\Delta_{30°}(\infty)$.

For the B_{1g} configuration, we find a surprisingly good match between A_{AR} and $A_{B_{1g}}$ in the low fluence[19] region, where the SC gap is only partially suppressed. At higher $\mathcal{F}$, where the gap[20] is completely suppressed, the dynamics appears significantly different below ~3 ps, unless we compare curves with very different fluences. Ignoring the response function, a direct comparison of $\Delta_{30°}$ at $\mathcal{F} = 23$ μJ/cm^2 to $A_{B_{1g}}$ at 4.4 times higher $\mathcal{F} = 102$ μJ/cm^2 gives a good match in the region of the strong suppression of the gap.

For the A_{1g}-dominated configuration, a better match is observed when we compare A to $\Delta_{30°}$ directly [Fig. 8(d)] while A_{AR} shows consistently higher magnitude than A. Similarly to the B_{1g} configuration, a good match is observed at a complete SC gap suppression between the TR-ARPES trajectory at $\mathcal{F} = 15$ μJ/cm^2 and A at 4.5 times higher $\mathcal{F} = 68$ μJ/cm^2.

Assuming that the TR-ARPES SC gap dynamics *is identical to the bulk gap* dynamics, the difference between the fluences of the corresponding-time-scales data can be at least partially attributed to the smearing of the optical-probe dynamics due to the depth-dependent excitation density and SC gap suppression. This is corroborated by the convergence of the optical and TR-ARPES trajectories with similar fluence on longer time scales, when the spatial inhomogeneity is expected to decrease.

The inaccuracy of the empirical response function [Fig. 8(b)] can further contribute to the difference, especially in the region of small SC order parameter. Contrary to LSCO [18] where the response function is linear up to $A_S \sim 0.8$, the s shape of the response function in the present case suggests that A_{AR} might be underestimated for low values of the gap.

Importantly, taking into account the inherent differences between the techniques, we can conclude that the TR-ARPES Fermi-arc SC gap and the antinodal SC gap inferred from

[17]The optical penetration depth in Bi-2212 is from optical data [33] ~200 nm at 1.55 eV and ~250 nm at 3.1 eV in comparison to a nm-scale photoelectron escape depth.

[18]The B_{1g} optical response is sensitive to a broad region near the antinode while the A_{1g} response samples both the nodal and antinodal regions [13].

[19]Due to the exponential decay of the excitation fluence away from the surface, the equivalent external fluence in all-optical experiment is ~1.5 times larger than in the case of TR-ARPES.

[20]The surface gap in the case of TR-ARPES and the bulk gap in the case of optics.

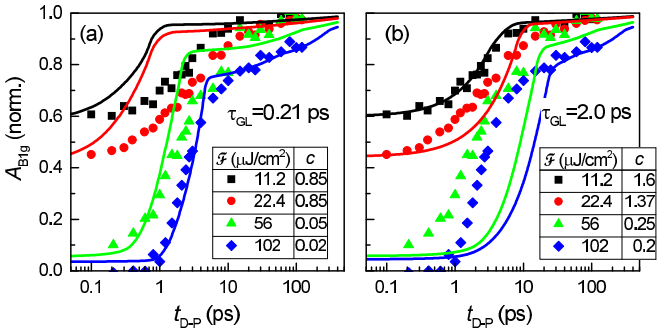

FIG. 9. Comparison of the simulated amplitude of the transient superconducting response to the B_{1g} experimental data measured at 15 K. (a), (b) Correspond to different values of τ_{GL} indicated in the graphs. Tables show the values of the parameter c defining the initial order parameter [Eq. (2)].

the B_{1g} channel multipulse optical probe show qualitatively identical suppression and recovery dynamics.

2. *Simulations*

As in the case of LSCO [18], we simulate the evolution of the order parameter through the transition by solving the dimensionless form of the first of the two TDGL equations:

$$\frac{\partial \psi}{\partial t} = \alpha_r(t,z)\psi - \psi|\psi|^2 + \nabla^2\psi, \tag{4}$$

where time and length are measured in units of τ_{GL} (fit parameter) and the coherence length, respectively. $\alpha_r(t,z)$ is a time- and depth-dependent reduced temperature which is the solution of the three temperature models [23] combined with the heat diffusion equation [18].

We neglect the second TDGL equation and any lateral variation of the order parameter, assuming that all the Kibble-Zurek (KZ) physics [30,31] can be phenomenologically absorbed into the initial order parameter $\psi_{BC}(z)$ using (2), and the phase dynamics, i.e., the dynamics of vortices, does not significantly modify the order-parameter amplitude.

Moreover, contrary to LSCO, where the PG order remains unsuppressed up to high excitation fluences [25], in Bi-2212 the PG order parameter is suppressed at lower excitation densities and can couple to the SC order parameter [15]. The PG order in Bi-2212 remains unsuppressed and time independent up to $\mathcal{F}_D \sim 50\ \mu J/cm^2$ and recovers on the subpicosecond time scale [19] at higher fluences [see Figs. 5(a)–5(c)]. In our data, we observe virtually no SC order recovery on the sub-picosecond time scale for $\mathcal{F}_D \gtrsim 50\ \mu J/cm^2$. The PG order parameter can be therefore considered time independent in the region $\{\mathcal{F}_D \lesssim 50\mu J/cm^2\} \cup \{t_{D\text{-}P} \gtrsim 1\ ps\}$ where the nonstationary SC order is observed (and calculated) and contributes only to the static renormalization of the parameters in (4) and (2).

The two fitting parameters c [Eq. (2)] and τ_{GL} are rather independent. While the first defines the Kible-Zurek-physics–related amplitude of the response at $t = 0$, the second defines the time scale of the recovery. In Fig. 9 we present typical results of the simulations for two different values of the τ_{GL} optimized to fit the highest-$\mathcal{F}_D$ and the lowest-$\mathcal{F}_D$ trajectories at 15 K, respectively. One can see that while a decent agreement for a targeted curve can be achieved, one needs to significantly vary τ_{GL} to fit the complete data set. Since such variation is unphysical, we can state that the presented TDGL approach is only sufficient to describe the present data qualitatively, contrary to what was found in LSCO, where a more quantitative description is possible.

The lack of quantitative description can not be attributed to the omission of the second TDGL equation and the resulting vortex dynamics it describes. While at a partial SC state order-parameter suppression no KZ vortices formation is expected, more vortices would be created with further suppression. The presence of vortices at increased order-parameter suppression is expected to further slow down the SC state recovery.[21] Looking at Fig. 9, one can clearly see that even without the vortex dynamics the TDGL solutions display a stronger recovery-time-scale slowdown with increased order-parameter suppression than the experimental data, so inclusion of the vortex dynamics into modeling is expected to only increase the discrepancy.

On the other hand, the lack of quantitative description is not very surprising due to the large pairing fluctuations contribution [29] to the transient reflectivity above T_c that prevents strict applicability of the TDGL theory and undermine the phenomenological link between the order-parameter magnitude and the experimentally observable A_S.

V. SUMMARY AND CONCLUSIONS

Our systematic investigation of the ultrafast optical suppression and recovery of the superconducting state in $Bi_2Sr_2CaCu_2O_{8+\delta}$ by means of polarization-selective multipulse optical time-resolved spectroscopy leads to some interesting, and somewhat surprising, findings. We found that the SC order is suppressed on the 200-fs time scale, comparable to the recent laser TR-ARPES [10] results. The destruction time scale is independent of the temperature and optical destruction pulse energy and is consistent with a photoexcited carrier energy transfer to the high-energy pair-breaking phonons.

The recovery of the SC order is slower appearing on the 2–8 ps time scale showing nonmonotonous dependence on the destruction pulse energy. At low T and a partial SC state suppression, the data show that the SC gap in the antinodal region recovers faster than near the nodes. Perhaps surprisingly, the recovery also slows down with decreasing T highlighting the importance of thermal fluctuations in the recovery mechanism. When the SC state is strongly suppressed, the recovery becomes nonexponential with the recovery time scale slowing down, becoming T independent. The fact that the antinodal SC order-parameter recovery dynamics inferred from the B_{1g} channel and the TR-ARPES Fermi-arc SC gap dynamics [10] show qualitatively identical recovery dynamics gives us confidence in the significance of the multipulse technique.

Despite strong SC fluctuations above T_c and the anisotropic SC-gap recovery the time-dependent Ginzburg-Landau model qualitatively describes the SC order temporal dynamics reasonably well, considering its limitations.

[21] Supplemental Material to Ref. [18].

ACKNOWLEDGMENTS

The authors acknowledge the financial support of Slovenian Research Agency (research core funding Grant No. P1-0040) and European Research Council Advanced Grant TRAJECTORY (Grant No. GA 320602) for financial support. We would like to thank L. Stojchevska for helping with the measurements.

[1] Y. M. Bunkov and H. Godfrin, in *Topological Defects and the Non-Equilibrium Dynamics of Symmetry Breaking Phase Transitions*, edited by Y. M. Bunkov and H. Godfrin (Springer Netherlands, Dordrecht, 2000), p. 396.
[2] P. W. Higgs, Phys. Rev. **145**, 1156 (1966).
[3] G. Volovik, *Contemporary Physics*, Vol. 5 (Oxford University Press, Oxford, 2010), pp. 451–452.
[4] M. Carnahan, R. Kaindl, J. Orenstein, D. Chemla, S. Oh, and J. Eckstein, Phys. C (Amsterdam) **408**, 729 (2004).
[5] P. Kusar, V. V. Kabanov, J. Demsar, T. Mertelj, S. Sugai, and D. Mihailovic, Phys. Rev. Lett. **101**, 227001 (2008).
[6] C. Giannetti, G. Coslovich, F. Cilento, G. Ferrini, H. Eisaki, N. Kaneko, M. Greven, and F. Parmigiani, Phys. Rev. B **79**, 224502 (2009).
[7] Y. Toda, T. Mertelj, P. Kusar, T. Kurosawa, M. Oda, M. Ido, and D. Mihailovic, Phys. Rev. B **84**, 174516 (2011).
[8] M. Beyer, D. Städter, M. Beck, H. Schäfer, V. V. Kabanov, G. Logvenov, I. Bozovic, G. Koren, and J. Demsar, Phys. Rev. B **83**, 214515 (2011).
[9] C. L. Smallwood, J. P. Hinton, C. Jozwiak, W. Zhang, J. D. Koralek, H. Eisaki, D.-H. Lee, J. Orenstein, and A. Lanzara, Science **336**, 1137 (2012).
[10] C. L. Smallwood, W. Zhang, T. L. Miller, C. Jozwiak, H. Eisaki, D.-H. Lee, and A. Lanzara, Phys. Rev. B **89**, 115126 (2014).
[11] C. L. Smallwood, W. Zhang, T. L. Miller, G. Affeldt, K. Kurashima, C. Jozwiak, T. Noji, Y. Koike, H. Eisaki, D.-H. Lee *et al.*, Phys. Rev. B **92**, 161102 (2015).
[12] C. Piovera, Z. Zhang, M. d'Astuto, A. Taleb-Ibrahimi, E. Papalazarou, M. Marsi, Z. Z. Li, H. Raffy, and L. Perfetti, Phys. Rev. B **91**, 224509 (2015).
[13] T. P. Devereaux and R. Hackl, Rev. Mod. Phys. **79**, 175 (2007).
[14] Y. Toda, F. Kawanokami, T. Kurosawa, M. Oda, I. Madan, T. Mertelj, V. V. Kabanov, and D. Mihailovic, Phys. Rev. B **90**, 094513 (2014).
[15] G. Coslovich, C. Giannetti, F. Cilento, S. Dal Conte, T. Abebaw, D. Bossini, G. Ferrini, H. Eisaki, M. Greven, A. Damascelli, and F. Parmigiani, Phys. Rev. Lett. **110**, 107003 (2013).
[16] V. V. Kabanov, J. Demsar, B. Podobnik, and D. Mihailovic, Phys. Rev. B **59**, 1497 (1999).
[17] R. Yusupov, T. Mertelj, V. V. Kabanov, S. Brazovskii, P. Kusar, J.-H. Chu, I. R. Fisher, and D. Mihailovic, Nat. Phys. **6**, 681 (2010).
[18] I. Madan, P. Kusar, V. V. Baranov, M. Lu-Dac, V. V. Kabanov, T. Mertelj, and D. Mihailovic, Phys. Rev. B **93**, 224520 (2016).
[19] I. Madan, T. Kurosawa, Y. Toda, M. Oda, T. Mertelj, and D. Mihailovic, Nat. Commun. **6**, 6958 (2015).
[20] R. Cortés, L. Rettig, Y. Yoshida, H. Eisaki, M. Wolf, and U. Bovensiepen, Phys. Rev. Lett. **107**, 097002 (2011).
[21] L. Stojchevska, P. Kusar, T. Mertelj, V. Kabanov, Y. Toda, X. Yao, and D. Mihailovic, Phys. Rev. B **84**, 180507(R) (2011).
[22] See, for example, Eq. (3) in Ref. [32].
[23] L. Perfetti, P. A. Loukakos, M. Lisowski, U. Bovensiepen, H. Eisaki, and M. Wolf, Phys. Rev. Lett. **99**, 197001 (2007).
[24] V. V. Kabanov, J. Demsar, and D. Mihailovic, Phys. Rev. Lett. **95**, 147002 (2005).
[25] P. Kušar, V. V. Kabanov, S. Sugai, J. Demšar, T. Mertelj, and D. Mihailović, J. Supercond. Novel Magnet. **24**, 421 (2011).
[26] P. Kusar, Influence of irregularities and dimensionality on electron relaxation, Ph.D. thesis, Faculty of Mathemathics and Physics, University of Ljubljana, Slovenia, 2007.
[27] C. L. Smallwood, T. L. Miller, W. Zhang, R. A. Kaindl, and A. Lanzara, Phys. Rev. B **93**, 235107 (2016).
[28] W. Zhang, C. L. Smallwood, C. Jozwiak, T. L. Miller, Y. Yoshida, H. Eisaki, D.-H. Lee, and A. Lanzara, Phys. Rev. B **88**, 245132 (2013).
[29] I. Madan, T. Kurosawa, Y. Toda, M. Oda, T. Mertelj, P. Kusar, and D. Mihailovic, Sci. Rep. **4**, 5656 (2014).
[30] T. W. B. Kibble and G. E. Volovik, J. Exp. Theor. Phys. Lett. **65**, 102 (1997).
[31] W. Zurek, Phys. Rep. **276**, 177 (1996).
[32] T. Mertelj, P. Kusar, V. V. Kabanov, L. Stojchevska, N. D. Zhigadlo, S. Katrych, Z. Bukowski, J. Karpinski, S. Weyeneth, and D. Mihailovic, Phys. Rev. B **81**, 224504 (2010).
[33] J. Hwang, T. Timusk, and G. Gu, J. Phys.: Condens. Matter **19**, 125208 (2007).